Energy Technology
Generation, Conversion, Storage, Distribution
www.entechnol.de

Delamination of Perovskite Solar Cells in Thermal Cycling and Outdoor Tests

Ulas Erdil, Mark Khenkin, Wander Max Bernardes de Araujo, Quiterie Emery, Iver Lauermann, Vasiliki Paraskeva, Matthew Norton, Sudhakar Vediappan, D. Kishore Kumar, Ritesh Kant Gupta, Iris Visoly-Fisher, Maria Hadjipanayi, George E. Georghiou, Rutger Schlatmann, Antonio Abate, Eugene A. Katz, and Carolin Ulbrich*

For the commercialization of perovskite solar cells (PSCs), detection of associated degradation mechanisms and mitigation of their effect is of paramount importance. The former requires outdoor and indoor stability tests to detect these mechanisms under real operation conditions and to accelerate them under controlled environments. Herein, the thermomechanical stability of encapsulated PSCs in outdoor tests at three locations coupled with indoor thermal cycling tests is investigated. Results show that encapsulant-induced partial delamination can occur in outdoor and indoor tests, leading to disruption in device integrity and substantial loss in the cell active area and short-circuit current. The findings suggest that delamination involves C_{60} and SnO_2 layers as the mechanically weakest point in the device stack. To the best of our knowledge, this work is the first demonstration of delamination in encapsulated PSCs under real operation conditions. While partial delamination emerged on some of the cells exposed in Israel and Cyprus in just a few weeks, it did not occur in Germany over 2.5 years of outdoor exposure. This highlights the importance of multiclimate outdoor testing to validate the significance of failure modes observed through accelerated indoor testing.

1. Introduction

In recent years, tremendous progress has been achieved in the efficiency and upscaling of perovskite-based solar cells.[1,2] However, the stability of these cells persists as the primary obstacle in the transformation from lab technology to a commercial product.[3] The stability of PSCs can be affected by oxygen, moisture, light, mechanical stress, and bias, all of which build the environment where PSCs are meant to operate eventually.[4] Consequently, outdoor stability tests combined with indoor accelerated ones are a must to investigate degradation mechanisms.[5] The frameworks of such stability tests for PSCs were adopted from the International Summit on Organic Photovoltaic Stability (ISOS) protocols and serve as a guideline for the stability studies of PSCs.[6]

The real-world operation of PSCs requires meticulous device packaging, especially to prevent oxygen and moisture ingresses, which lead to premature failures.[7,8] However, even this protective measure can have its own trade-offs. Notably, encapsulant-related failures are the most frequent failure modes observed in the field for commercial photovoltaic (PV) technologies, and delamination, a failure involving detachment of layers, is a commonly encountered issue.[9] In multilayered devices, delamination is primarily caused by thermal expansion coefficient mismatch between

U. Erdil, M. Khenkin, W. M. Bernardes de Araujo, Q. Emery, I. Lauermann, R. Schlatmann, A. Abate, C. Ulbrich
Helmholtz-Zentrum Berlin für Materialien und Energie
Hahn-Meitner-Platz 1, 14109 Berlin, Germany
E-mail: mark.khenkin@helmholtz-berlin.de

U. Erdil, A. Abate
Faculty of Chemistry
Bielefeld University
33615 Bielefeld, Germany

The ORCID identification number(s) for the author(s) of this article can be found under https://doi.org/10.1002/ente.202401280.

DOI: 10.1002/ente.202401280

V. Paraskeva, M. Norton, M. Hadjipanayi, G. E. Georghiou
FOSS Research Centre for Sustainable Energy
Department of Electrical and Computer Engineering
University of Cyprus
77 Kallipoleos St., 1678 Nicosia, Cyprus

S. Vediappan, D. K. Kumar, R. K. Gupta, I. Visoly-Fisher, E. A. Katz
Ben-Gurion National Solar Energy Center
Swiss Institute for Dryland Environmental and Energy Research
Jacob Blaustein Institutes for Desert Research
Ben-Gurion University of the Negev
Midreshet Ben-Gurion 84990, Israel

R. Schlatmann
Faculty 1 – Energy and Information
Hochschule für Technik und Wirtschaft Berlin
10313 Berlin, Germany

contiguous layers and geometric discontinuities, which act as stress concentration points.[10] Furthermore, encapsulation process-related defects can exacerbate delamination.[11] Likewise, delamination in PV modules mainly arises at the encapsulant–cell interface, particularly at cell metallization.[12] Given its disruptive nature, it usually manifests as bubbles or blisters; hence, it can mostly be detected by the naked eye and results in current loss, which can roughly correlate with the delaminated area.[13,14]

Previously, only a few studies investigated delamination in perovskite-based solar cells. Cheacharoen et al. compared the mechanical stability of PSCs with Surlyn and ethylene vinyl acetate (EVA) encapsulants through temperature cycling, in which stiff Surlyn caused delamination.[15] They suggested that the delamination originates at PCBM, a fullerene-based electron transport layer (ETL), as it has the lowest fracture energy in the cell stack. Bastiani et al. investigated delamination in perovskite/silicon tandem solar cells by controlled peel-off of the top electrode.[16] They found that the C_{60}/SnO_2 interface is the origin of the delamination due to weakened adhesion between these layers throughout cell processing. However, to the best of our knowledge, such delamination has not yet been examined and reported in perovskite-based solar cells under real operation conditions.

In this work, we investigated the thermomechanical stability of state-of-the-art-encapsulated PSCs through outdoor tests at three different climates, as well as indoor thermal cycling tests. We observed that encapsulant-induced partial delamination tends to occur more in harsher climates, leading to interruption of charge transport and, thus, significant current losses. The failure mechanism was reproduced by the indoor thermal cycling test, which enabled the determination of performance losses due to delamination as well as insights into the dynamics of the phenomenon. Our findings suggested that delamination arises from an interplay between mechanical constraints, uncontrolled manufacturing flaws, and climatic factors. The latter was highlighted by the fact that delamination was the predominant degradation mechanism in Israel and Cyprus, while it did not occur in Germany.

2. Results and Discussion

PSCs were fabricated with a layer stack of glass/ITO/2PACz/perovskite/C_{60}/SnO_2/Cu, as shown in **Figure 1**a. Each substrate contained six individual solar cells, labeled from 1 to 6 (Figure 1b). We used polyolefin (POE) as an encapsulant, which demonstrated superior stability at both indoor and outdoor stability tests in previous studies.[17,18] Each substrate was encapsulated by sandwiching it between two glasses with a butyl edge sealant and POE encapsulant with ribbons as electrical contacts inside the encapsulation, as depicted in Figure 1c. Outdoor tests were conducted following ISOS-O protocols at three locations: Berlin, Germany; Nicosia, Cyprus; and the Negev Desert, Israel, representing climates ranging from warm temperate, through steppe, to desert.[19] Due to technicalities, different subcategories of ISOS-O protocols were implemented at the test locations. We believe slight technical differences in experimental setups do not affect the discussion here. In total, 9 substrates with 54 individual perovskite solar cells (PSCs) were tested across these locations. In the context of delamination, we will refer to the number of substrates affected rather than the number of individual cells, as the delamination process might be influenced by forces acting at the substrate level rather than the cell level. It should be noted that the delamination observed in this work occurs locally and, therefore, does not affect all the cells on the substrate equally. An overview of implemented protocols and assigned substrates at testing locations is given in Table S1, Supporting Information. For indoor thermal cycling tests, we implemented the ISOS-T-3 protocol, where the temperature is cycled between −40 and 85 °C in the dark.

2.1. Outdoor Tests

At outdoor tests in Israel and Cyprus, some cells were affected by delamination within approximately the first two weeks of exposure, leading to current losses as evident from their current density–voltage (J–V) curves (**Figure 2**a–d). In Israel, the current losses were immediately matched with blisters on the copper electrode, as photographed in Figure 2b. After the 3 month-long outdoor operation, these blisters were better visualized via photoluminescence (PL) imaging (Figure 2c) and revealed a correlation between the delaminated area and current loss. In Cyprus, blisters also appeared on the electrodes of the cells (Figure 2e–f). In this case, both the photograph and PL image were obtained after the 5 month-long outdoor operation; therefore, correlating delaminated areas to current losses is not feasible, but the overall

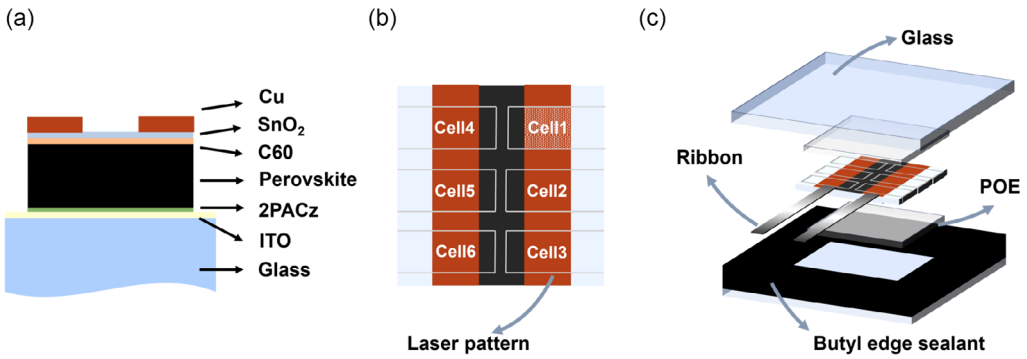

Figure 1. Schematic of cell layout, substrate geometry, and encapsulation. a) Schematic cross-sectional view of the layer stack. b) Top view of the substrate. Gray lines indicate laser patterns on the ITO layer, which electrically isolate six cells from each other. The patterned background of Cell1 represents the cell active area (0.16 cm^2) defined as an overlap between ITO and metal electrode. c) Encapsulation stack.

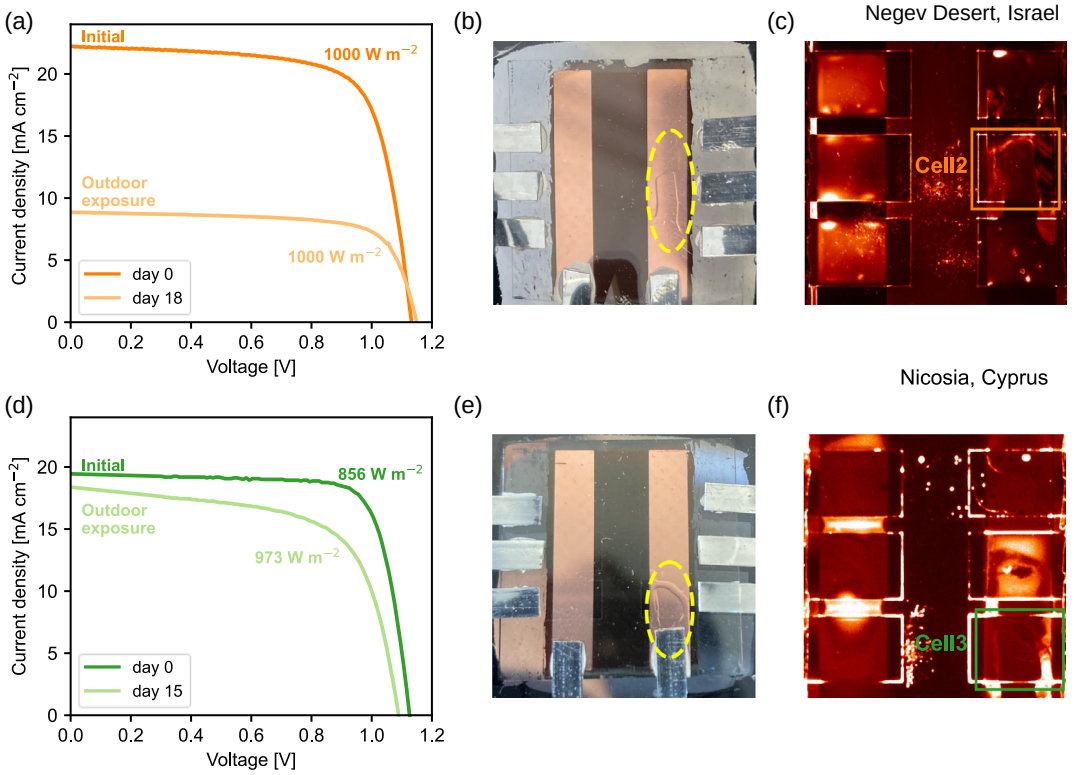

Figure 2. Delamination at outdoor tests in Israel (top row) and Cyprus (bottom row). a,d) *J–V* curves of cells affected by delamination. *J–V* measurements in Israel were conducted under sun simulator, whereas in Cyprus, they were done under natural sunlight. Therefore, global normal irradiance values were given together with the corresponding curves. b,e) Photographs of delaminated substrates; b) captured after 18 days, whereas e) captured after five months of outdoor operation. c,f) PL images of the same substrates. c) was taken after three months, whereas f) taken after five months of outdoor operation.

pattern of observations is very similar. Generally, the decrease in the short-circuit current (J_{SC}) for a delaminated cell strongly depends on the extent of the delamination within that cell, as will be discussed later. This variation accounts for the significant differences in apparent degradation rates observed in the examples shown in Figure 2.

It is noteworthy to mention that outdoor tests involve a multi-stress environment. Hence, PSCs can simultaneously undergo several degradation/failure mechanisms, which can influence different cell parameters. For instance, decreased shunt resistance in Cell2 after two weeks of outdoor operation in Cyprus was not caused by delamination, as this type of degradation was also observed for nondelaminated cells (Figure S1, Supporting Information), and its origin is beyond the scope of this study. Consequently, the coexistence of several degradation modes in the same device makes the analysis of outdoor degradation challenging. For this reason, it is imperative to direct the effort of the research community to separate individual degradation mechanisms by their observable features, as is done in this work for partial delamination.

Although we observed delamination in one of two substrates that were tested outdoors in Israel and Cyprus, no delamination has been observed in the five substrates that have been operating outdoors in Germany for durations ranging from 1 to 2.5 years. Additionally, we recently demonstrated the outdoor performance of various single-junction PSCs in Berlin using the same encapsulation scheme depicted in Figure 1c.[20] Notably, no delamination failures were observed in these devices either. Therefore, it was unexpected to observe this degradation phenomenon within the first weeks of outdoor experiments conducted in hot climates. Although the limited number of cells tested precludes establishing a probability of failure for each climate, the data clearly demonstrate that delamination can manifest under real-world conditions.

To analyze these contrasting outcomes in different climates, we calculated diurnal cell temperature (T_{cell}) variations (the difference between the daily maximum and minimum cell temperature, see Note 1, Supporting Information) at these locations. **Figure 3** demonstrates that the diurnal T_{cell} variations in Israel and Cyprus are only slightly above those observed for substrates exposed in Germany during the summer period. This suggests that the magnitude of the diurnal T_{cell} variations is not the sole factor driving the delamination failure. A combination of environmental factors, such as the rate and frequency of temperature swings as well as humidity, might influence the probability of this failure mode. However, we were unable to establish a correlation between other environmental factors and the observed delamination, and their contributions remain undetermined at this stage. Nevertheless, the complexity of these interactions underscores

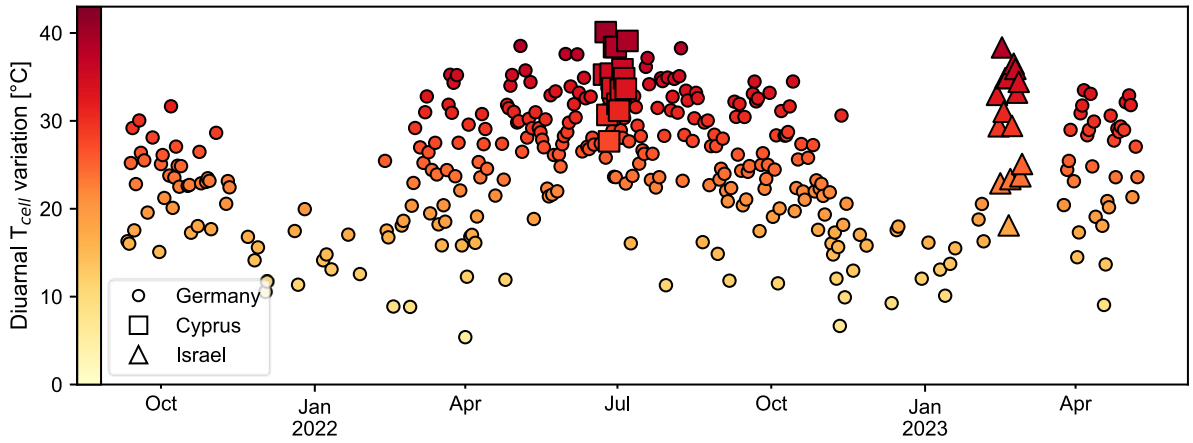

Figure 3. Comparison of calculated diurnal cell temperature variations in Cyprus (squares) and Israel (triangles) until detection of delamination, juxtaposed with the data spanning 18 months from Germany (circles) where no delamination was observed. For Germany, only days with average irradiance values exceeding 250 W m^{-2} between 12:00 and 13:00 were selected to filter out very low diurnal T_{cell} variations.

the importance of gathering experimental data across various climatic conditions.

2.2. Indoor Thermal Cycling Test

We performed indoor thermal cycling tests to simulate temperature fluctuations that PSCs experience during outdoor operation, thereby aiming to accelerate delamination. Notably, among various stress tests we conducted, including exposure to fixed elevated temperatures in the dark, damp heat, constant light at elevated temperatures, elevated light intensity, and electrical bias, only thermal cycling successfully induced delamination, closely resembling the results observed in the outdoor tests shown in Figure 2. **Figure 4**a shows the applied temperature profiles. After a few cycles, delamination was observed on some cells as a distinct pattern on the copper electrode, as captured in Figure 4b. Electroluminescence (EL) images of the cells provide enhanced clarity in visualizing this pattern and enable calculating the affected area via image processing (see Note 2, Supporting Information). The calculated dark areas (i.e., areas without EL signal) within each cell show an overall correlation with the decrease in J_{SC} in each cell throughout the cycles.

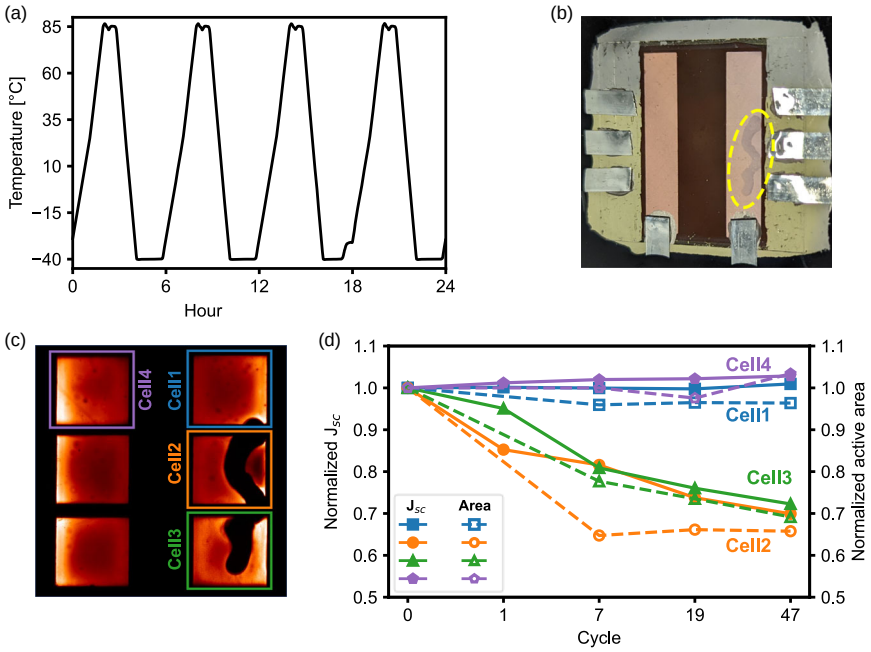

Figure 4. Delamination at indoor thermal cycling test. a) Temperature profile applied in the test. b) Photograph of the delaminated substrate. The yellow dashed line highlights the delaminated area. c) EL image of the delaminated substrate after 19 cycles, featuring six cells, with the delaminated area appearing dark due to lack of contact between perovskite bulk and transport layers. d) Evolution of normalized J_{SC} and normalized active area. Both were normalized to the initial respective values.

In contrast, a nondelaminated cell, Cell4, shows no J_{SC} or area losses (Figure 4d).

Conducting elemental analysis on observed delaminated regions presents significant experimental challenges due to the necessity of disassembling the encapsulated device stack, which is likely to cause additional mechanical damage beyond the delamination we intend to study. Therefore, to further investigate where the delamination occurred in the cell stack, we manually peeled off the copper electrode of an unencapsulated device with a Kapton tape. Subsequently, we analyzed the remaining surfaces on both tape (**Figure 5**a) and substrate (Figure 5b) using X-ray photoelectron spectroscopy (XPS), which offers a depth of analysis of ≈5 nm. Figure 5c shows the XPS spectrum on both surfaces. Besides anticipated peaks, we did not observe apparent traces of elements originating from the perovskite absorber or copper electrode on the tape side. This suggests delamination occurred within ETLs (C_{60}/SnO_2) covering the copper electrode left on the tape, preventing its detection. When the substrate was surveyed, characteristic peaks of perovskite components, for example, I3*d* (Figure 5d) and Pb4*f* (Figure 5e), appeared. This indicates that the delamination crack, at least at some point, extended to the perovskite/C_{60} interface, unveiling the perovskite absorber and allowing its detection. Note that observed indium and gold peaks originate from the scratched edge of the substrate and gold foil at the one edge of the manipulator head, respectively. Therefore, they are not relevant to the delamination process described here.

Manually peeling off the copper electrode does not necessarily reproduce the delamination process induced by temperature cycles. Nevertheless, these findings clarify the details of the delamination process. In particular, it helps rationalize minor discrepancies between J_{SC} and the cell active area observed for Cell1 and Cell2 in Figure 4d. Cell1 shows a slight delamination on the edge with no loss in J_{SC}, whereas Cell2 exhibits a substantial delaminated area without an immediate proportional decrease in current. In contrast, Cell3 demonstrates a strong correlation between these two. We speculate that the delamination initiated at the C_{60}/SnO_2 interface within Cell1, allowing the light-generated charge carriers to still be extracted from the cell due to the intact C_{60} layer, yet disrupted contact between C_{60} and SnO_2, created a very high series resistance preventing effective charge carrier injection into the affected area of the cell, leading to the dark area on the EL image. While propagating toward Cell2, delamination partially extended to the perovskite/C_{60} due to interface steps, specifically laser patterns, which can alter the propagation of delamination.[21] This led to the observed discrepancy within Cell2 because of intact C_{60} layer. At some point, the delamination crack substantially transferred to the perovskite/C_{60} interface and propagated at this interface in Cell3, resulting in a strong correlation between current loss and delaminated area. Further supporting this hypothesis, the initially observed discrepancy for Cell2 diminishes with cycles. This suggests that the interface crack slowly intruded into intact parts of C_{60} within the cell through continuous cycling stress, leading to its gradual disassociation, thus increasingly impaired charge transport. Moreover, some newly formed delaminated areas on Cell3 after 47 cycles show different contrast compared to previously delaminated areas in EL images (Figure S5, Supporting Information), further demonstrating the complex propagation of delamination.

Contrary to previous reports where the propagation of delamination crack was proposed within the fullerene layer[15] or at the fullerene/buffer layer interface,[16] our findings suggest that delamination crack can originate at the C_{60}/SnO_2 interface but can travel across C_{60} due to device geometries and continuous stress. Nonetheless, it is evident that fullerene-based layers play an adverse role in the delamination of PSCs, which is mainly attributed to their very low fracture energy.[22] Therefore, one of the approaches to overcome this failure mode would be to find suitable alternative ETL materials. Some of the fullerene derivatives have already been shown to have a much higher fracture resistance, but the solar cells combining favorable mechanical properties with high efficiency are yet to be demonstrated.[22]

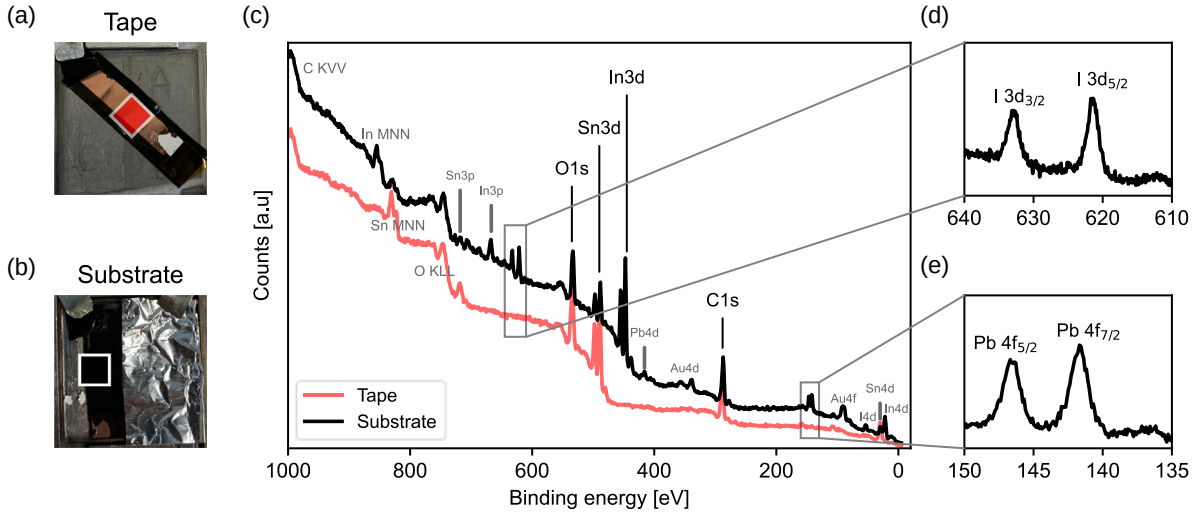

Figure 5. Manual peel-off test and XPS scans of emerged surfaces. Surfaces after manually peeling-off test, a) tape and b) substrate sides. c) XPS spectrum of scanned areas (1 cm^2) represented by red and black squares in a,b). Gray boxes show the zoomed-in characteristic peaks of d) I3*d* and e) Pb4*f*, which are related to the perovskite layer and appear only on the substrate side.

During indoor thermal cycling and outdoor tests, we observed instances where delamination occurred and instances where it did not, despite the tested devices being nominally identical. This is not surprising because commercial PV technologies sometimes experience delamination in the field, even though they pass rigorous qualification and type approval tests, including thermal cycling tests. This is sometimes attributed to issues with the encapsulation process.[9,23] It is well known that factors such as improper encapsulant curing, improper vacuum, voids, contaminants, etc. can influence delamination.[11,13] We performed our lamination process on many dozens of substrates. In some rare cases, we observed delamination directly after encapsulation, emphasizing the influence of the lamination process on the phenomenon. Consequently, we hypothesize that manufacturing defects beyond our control could also influence the likelihood of the observed partial delamination. On the other hand, it's important to consider the role of encapsulant material in delamination, urging more detailed studies that go beyond the moisture/oxygen barrier properties. For instance, a POE encapsulant designed for PV modules demonstrated increased peel strength through the incorporation of a polymer and additives.[24]

3. Conclusion

This study shows that encapsulant-induced partial delamination is a critical failure mechanism in state-of-the-art encapsulated PSCs under real operation conditions. Among several stress tests we performed, only the indoor thermal cycling test reproduced the observed delamination, highlighting the primary role of temperature fluctuations in the phenomenon. However, the variability of delamination occurrence in both outdoor and indoor tests suggests a complex interplay between environmental factors, mechanical constraints, and manufacturing flaws. Observed partial delamination appears as distinct patterns on the copper electrode, translating to detached areas of ETLs, thereby resulting in a proportional drop in current. Our findings also point out C_{60} as the mechanically weakest link in the cell stack. Although we did not observe any delamination in Berlin during 2.5 years of outdoor testing, cells failed within a few weeks due to delamination in Cyprus and Israel, emphasizing the importance of multiclimate studies when evaluating the field relevance of certain degradation modes. Coupled with the notion that shear stresses will increase with the scale-up of lab-scale PSCs,[25] encapsulant-induced delamination is expected to be a prevalent mechanism at the module level without further development of the currently most popular materials. Therefore, this work calls for further research to mitigate the issue on the way of commercialization.

4. Experimental Section

Cell Fabrication and Encapsulation: ITO-coated glass substrates (Automatic Research GmbH) were consecutively sonicated in a 2% mucasol–water solution, deionized water, acetone, and isopropanol in an ultrasonic bath. Each step was for 15 min. Next, the substrates were treated with a UV–ozone cleaner for 15 min. 2PACz (1 mM, 100 µL) solution was spun on the substrates with a 5-s acceleration to 3000 rpm and subsequent spinning for 30 s. Following, the films were annealed at 100 °C for 10 min. For the perovskite absorber, $Cs_{0.17}FA_{0.83}PbI_{2.49}Br_{0.51}$ (1.3 M) with slightly excess PbI_2 was prepared by dissolving CsI (114.8 mg), FAI (371.1 mg), $PbBr_2$ (243.3 mg), and PbI_2 (901.9 mg) in a DMF/DMSO (2000 µL, 4:1 vol%) solution. The perovskite solution (100 µL) was spun with a 5 s acceleration to 3500 rpm and subsequent spinning took place for 35 s. Anisole (250 µL) was dropped onto the spinning substrate 10 s before the process ended. Following, the films were annealed at 100 °C for 30 min. C_{60} was thermally evaporated until a 23 nm layer was achieved and followed by the deposition of a 20 nm SnO_2 layer via atomic layer deposition. The cell stack was completed by thermal evaporation of 100 nm copper using a mask to achieve a 0.16 cm^2 cell area. Encapsulation was performed as described elsewhere.[18]

Outdoor and Indoor Stability Tests: In Berlin, Germany (52°25'53.5"N, 13°31'27.7"E), outdoor tests were conducted on the roof-top setup where encapsulated PSCs were fixed on a 35° tilted stage oriented toward to the south. Maximum power point tracking system (MP2005M6, LPVO), employing a perturb and observe algorithm, was used to keep each cell at maximum power point. Irradiance in the plane of PSCs was recorded with an EKO ML-02 Si-pyranometer. The temperature inside the encapsulation was measured with a type K thermocouple placed in the lamination process. Environmental data were measured by the meteorology station (CLIMA SENSOR US 4.920x.00.00x) next to the outdoor testing setup. In Nicosia, Cyprus (35°8'46.4" N, 33°25'3.3" E) outdoor tests were conducted on a fixed, south-facing plane tilted at 32° to the horizontal. The cells were attached to a Keithley 2430 Source Meter using a four-wire Kelvin probe arrangement via a multiplexing system that would sequentially measure the devices. The irradiance in the plane of the devices under test was measured using a Hukseflux SR11 pyranometer. Environmental data including ambient temperature, humidity, wind speed, wind direction, and air pressure were recorded using various sensors connected to the FOSS PV Technology meteo data logging system. In Negev desert, Israel (30°51'25.5"N, 34°46'51.3"E), outdoor tests were performed on a fixed south-facing stage tilted at 29°. The irradiance in the plane of cells was measured with a thermopile pyranometer (EppleyPSP) placed on the same platform. The cells were connected to the maximum power point tracking system (MP2005M6, LPVO). Environmental data were measured by the Sede-Boker meteorological observation site. Indoor temperature cycling tests were carried out in an alternating climate chamber (MKFT 115, BINDER GmbH) where temperature cycled between −40 and 85 °C. The temperature cycles were programmed with chambers' own program controller.

Characterization: For indoor temperature cycling tests, *J–V* measurements were conducted under simulated AM1.5G spectrum with a 1 sun illumination by a calibrated dual-source solar simulator (WXS-155S-L, class AAA, Wacom) and a Keithley 238 SMU. Substrates were fixed on a temperature-controlled chuck that was kept at 25 °C. The voltage was swept in forward and reverse directions between −0.2 and 1.2 V, with steps of 0.01 V. Integration time and settling time were 20 and 40 ms, respectively. The corresponding cell parameters reported here were measured after 10 min of light soaking. In Cyprus, *J–V* measurements of cells under OC condition were conducted with monthly intervals under natural sunlight with the above-described electronics on the outdoor testing stage without temperature control. The voltage was swept in both directions between −0.2 and 1.2, with steps of 0.01 V, and settling time of 50 ms. In Israel, the *J–V* measurements were conducted under simulated AM1.5G spectrum with 1 sun illumination intensity by a solar simulator (LCS-100, class ABB, Newport) and a Keithley 2401 SMU. The voltage was swept in both directions between −0.2 and 1.2 V, with steps of 0.055 V, and settling time of 20 ms. EL and PL images were taken with a LumiSolarMobile System from GreatEyes equipped with a charge-coupled device (CCD) camera. Power was provided by programmable power supply (GEN1U1500W, TDK). For EL images, maximum current was 4 mA with integration times ranging between 700 and 1000 ms. For PL images, illumination was supplied by four 528 nm light-emitting diode blocks. A longpass filter with cuton wavelength of 700 nm was attached to the CCD camera. The integration time was 100 ms. XPS measurements were performed in the CISSY setup at HZB[26] using an XR-50 X-ray source from SPECS with Mg Kα anode (1253.6 eV) at a power of 150 W and a CLAM 4 electron analyzer from Vacuum Generators at a pass

energy of 20 eV. The electron spectrometer was calibrated using photoemission and Auger line position references of sputter-cleaned copper and gold samples according to established procedures.[27]

Supporting Information

Supporting Information is available from the Wiley Online Library or from the author.

Acknowledgements

U.E. is grateful for the support by the German-Israeli Helmholtz International Research School HI-SCORE (HIRS-0008) and Helmholtz Association within the project "Zeitenwende – Tandem Solarzellen." M.K. And C.U. acknowledge the support of the European partnering project TAPAS (PIE-0015). UCY and E.A.K. (BGU) acknowledges financial support by the European Union through the TESTARE project (grant id: 101079488). Additonally, UCY acknowledges the financial support by the European Regional Development Fund and the Republic of Cyprus through the DegradationLab project (grant id: INFRASTRUCTURES/1216/0043). V.S. is grateful for the Krietman Postdoctoral fellowship at BGU. D.K.K. is grateful for the Blaustein postdoctoral fellowship at BGU. R.K.G. is grateful for the Swiss Institute for Dryland Environmental and Energy Research postdoctoral fellowship at BGU.

Open Access funding enabled and organized by Projekt DEAL.

Conflict of Interest

The authors declare no conflict of interest.

Data Availability Statement

The data that support the findings of this study are available from the corresponding author upon reasonable request.

Keywords

delaminations, encapsulations, outdoors, perovskite solar cells stabilities, thermal cycling

Received: July 29, 2024
Published online: September 29, 2024

[1] Best Research-Cell Efficiency Chart, https://www.nrel.gov/pv/cell-efficiency.html (accessed: March 2024).
[2] Champion Photovoltaic Module Efficiency Chart, https://www.nrel.gov/pv/module-efficiency.html (accessed: March 2024).
[3] T. A. Chowdhury, A. B. Zafar, M. S. U. Islam, M. Shahinuzzaman, M. A. Islam, M. U. Khandaker, *RSC Adv.* **2023**, *13*, 1787.
[4] C. C. Boyd, R. Cheacharoen, T. Leijtens, M. D. McGehee, *Chem. Rev.* **2019**, *119*, 3418.
[5] M. Khenkin, S. Albrecht, *Nat. Energy* **2023**, *9*, 12.
[6] M. V. Khenkin, E. A. Katz, A. Abate, G. Bardizza, J. J. Berry, C. Brabec, F. Brunetti, V. Bulović, Q. Burlingame, A. Di Carlo, R. Cheacharoen, Y.-B. Cheng, A. Colsmann, S. Cros, K. Domanski, M. Dusza, C. J. Fell, S. R. Forrest, Y. Galagan, D. Di Girolamo, M. Grätzel, A. Hagfeldt, E. von Hauff, H. Hoppe, J. Kettle, H. Köbler, M. S. Leite, S. Liu, Y.-L. Loo, J. M. Luther, et al., *Nat. Energy* **2020**, *5*, 35.
[7] N. Aristidou, C. Eames, I. Sanchez-Molina, X. Bu, J. Kosco, M. S. Islam, S. A. Haque, *Nat. Commun.* **2017**, *8*, 15218.
[8] P. Tolueinia, H. Khassaf, A. Shirazi Amin, Z. M. Tobin, S. P. Alpay, S. L. Suib, *ACS Appl. Energy Mater.* **2020**, *3*, 8240.
[9] J. H. Wohlgemuth, P. Hacke, N. Bosco, D. C. Miller, M. D. Kempe, S. R. Kurtz, in *2016 IEEE 43rd Photovoltaic Specialists Conf. (PVSC)*, Portland **2016**.
[10] W.-S. Lei, A. Kumar, in *Adhesion in Microelectronics* (Eds: K. L. Mittal, T. Ahsan), John Wiley & Sons, Scrivener Publishing LLC, Hoboken, NJ, Salem, MA, USA **2014**, pp. 267–312.
[11] H. Ardebili, M. G. Pecht, in *Encapsulation Technologies for Electronic Applications*, William Andrew Publishing, Oxford **2009**.
[12] J. Tracy, N. Bosco, R. Dauskardt, *IEEE J. Photovoltaics* **2017**, *7*, 1635.
[13] R. Meena, A. Pareek, R. Gupta, *Renewable Sustainable Energy Rev.* **2024**, *189*, 113944.
[14] D. C. Jordan, T. J. Silverman, J. H. Wohlgemuth, S. R. Kurtz, K. T. VanSant, *Prog. Photovoltaics* **2017**, *25*, 318.
[15] R. Cheacharoen, N. Rolston, D. Harwood, K. A. Bush, R. H. Dauskardt, M. D. McGehee, *Energy Environ. Sci.* **2018**, *11*, 144.
[16] M. De Bastiani, G. Armaroli, R. Jalmood, L. Ferlauto, X. Li, R. Tao, G. T. Harrison, M. K. Eswaran, R. Azmi, M. Babics, A. S. Subbiah, E. Aydin, T. G. Allen, C. Combe, T. Cramer, D. Baran, U. Schwingenschlögl, G. Lubineau, D. Cavalcoli, S. De Wolf, *ACS Energy Lett.* **2022**, *7*, 827.
[17] R. Cheacharoen, C. C. Boyd, G. F. Burkhard, T. Leijtens, J. A. Raiford, K. A. Bush, S. F. Bent, M. D. McGehee, *Sustainable Energy Fuels* **2018**, *2*, 2398.
[18] Q. Emery, M. Remec, G. Paramasivam, S. Janke, J. Dagar, C. Ulbrich, R. Schlatmann, B. Stannowski, E. Unger, M. Khenkin, *ACS Appl. Mater. Interfaces* **2022**, *14*, 5159.
[19] H. E. Beck, N. E. Zimmermann, T. R. McVicar, N. Vergopolan, A. Berg, E. F. Wood, *Sci. Data* **2018**, *5*, 180214.
[20] M. Khenkin, H. Köbler, M. Remec, R. Roy, U. Erdil, J. Li, N. Phung, G. Adwan, G. Paramasivam, Q. Emery, E. Unger, R. Schlatmann, C. Ulbrich, A. Abate, *Energy Environ. Sci.* **2024**, *17*, 602.
[21] G. Parry, S. Hamade, J. Durinck, C. Coupeau, J. Colin, *J. Mech. Phys. Solids* **2019**, *132*, 103698.
[22] B. L. Watson, N. Rolston, K. A. Bush, T. Leijtens, M. D. McGehee, R. H. Dauskardt, *ACS Appl. Mater. Interfaces* **2016**, *8*, 25896.
[23] M. Aghaei, A. Fairbrother, A. Gok, S. Ahmad, S. Kazim, K. Lobato, G. Oreski, A. Reinders, J. Schmitz, M. Theelen, P. Yilmaz, J. Kettle, *Renewable Sustainable Energy Rev.* **2022**, *159*, 112160.
[24] B. Lin, C. Zheng, Q. Zhu, F. Xie, *J. Therm. Anal. Calorim.* **2020**, *140*, 2259.
[25] M. Dailey, Y. Li, A. D. Printz, *ACS Omega* **2021**, *6*, 30214.
[26] I. Lauermann, A. Steigert, *J. Large-Scale Res. Facil.* **2016**, *2*, A67.
[27] D. Briggs, M. P. Seah, in *Practical Surface Analysis, Auger and X-ray Photoelectron Spectroscopy*, Wiley, New York **1990**.